

Figure S1. **NMR data and structures of the INF2 2-36 and 2-19 free peptides.** (A) Bar plots of the difference of chemical shift values for α ^1H ($\Delta\delta_{\text{H}\alpha}$) and ^{13}C ($\Delta\delta_{\text{C}\alpha}$) as a function of the amino acid sequence of the 2-36 peptide in aqueous solution (black bars) and in 30% TFE (grey bars), and of 2-19 peptide in aqueous solution (red bars) and in 30% TFE (gold bars). The stretches of negative $\Delta\delta_{\text{H}\alpha}$ values and positive $\Delta\delta_{\text{C}\alpha}$ values indicate helix formation, as schematically shown in the cartoon between the two panels. RC, random coil value interval. (B) Ribbon representation of the ensemble of the 20 lowest target function conformers calculated for the INF2 2-36 peptide on the basis of NMR parameters. The conformers are overlaid onto the first helix (in red). The second helix is colored in magenta. (C) First helix of INF2 2-36: overlay of backbone atoms for residues 3-17 and ribbon representation of the first conformer of the ensemble. (D) Second helix of INF2 2-36: overlay of backbone atoms for residues 25-31 and ribbon representation of the first conformer of the ensemble. (E) Helix of INF2 2-19: overlay of backbone atoms and ribbon representation of the first conformer of the ensemble. (F) Overlay of the INF2 2-19 helix (red) onto the first helix of INF2 2-36 (black gray). Top panel: Backbone atoms of the 20 lowest target conformers of the two ensembles. Bottom panel: Ribbon representations of the first conformer of each ensemble. In panels (C-E), backbone atoms are shown in black. K and R side chains are displayed in blue, D and E side chains in red, and all others in green.

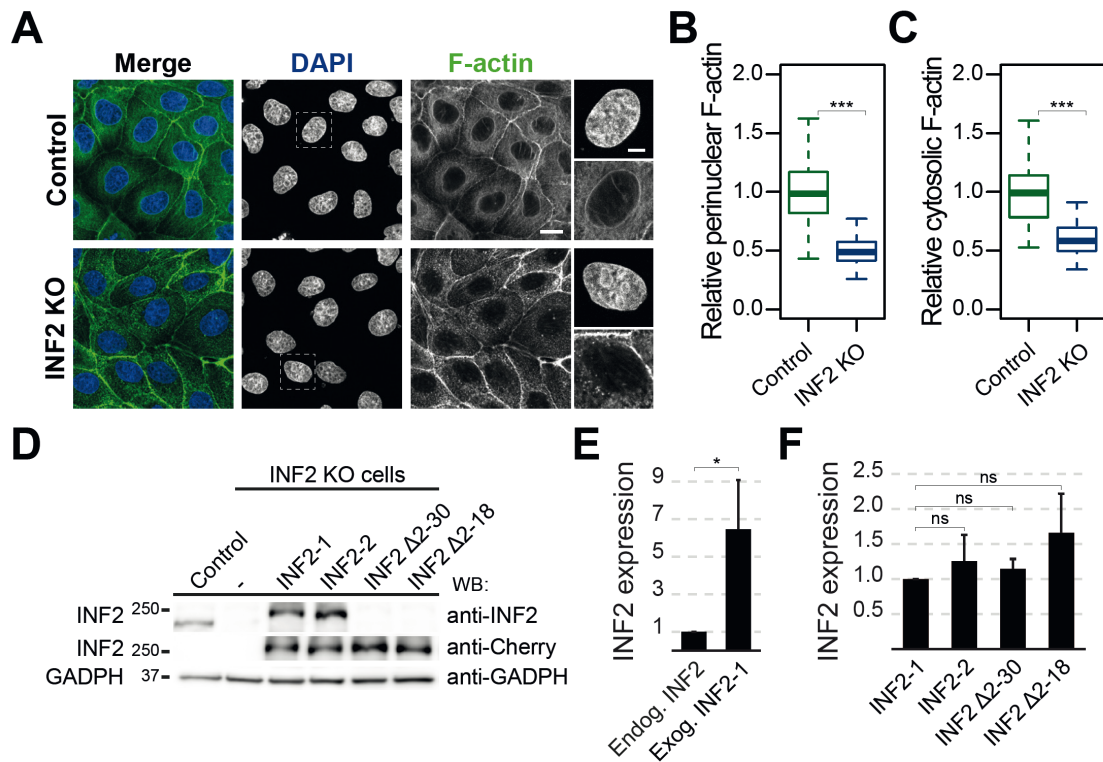


Figure S2. **Distribution of F-actin in INF2 KO cells and analysis of the levels of expression of exogenous INF2.** (A-C) Control and INF2 KO cells were stained for F-actin. Nuclei were visualized with DAPI. An enlargement of the DAPI and F-actin staining corresponding to the boxed regions is shown in the rightmost panels. Scale bars, 15 μm for the panoramic views and 5 μm for the enlargements (A). Box plots showing the intensity of F-actin staining at the perinuclear region (B) and the cytosol (C) relative to that of control cells (> 160 cells were examined for each experimental condition; three independent experiments; ***, $p < 0.001$). (D-F) The expression of endogenous INF2 in control wild type cells and that of the indicated exogenous INF2 proteins in INF2 KO cells were analyzed by immunoblotting with anti-antibodies that recognize both canine and human INF2 (top panel). The exogenous proteins were also analyzed with anti-Cherry antibodies (middle panel). The levels of GAPDH were taken as a loading control (bottom panel) (D). The graphs show the expression of exogenous INF2-1 relative to that of endogenous INF2 (E), and the expression of exogenous INF2-2, INF2 Δ 2-30 and INF2 Δ 2-18 relative to that exogenous INF2-1 (F). Three independent experiments; ns, not significant; *, $p < 0.05$).

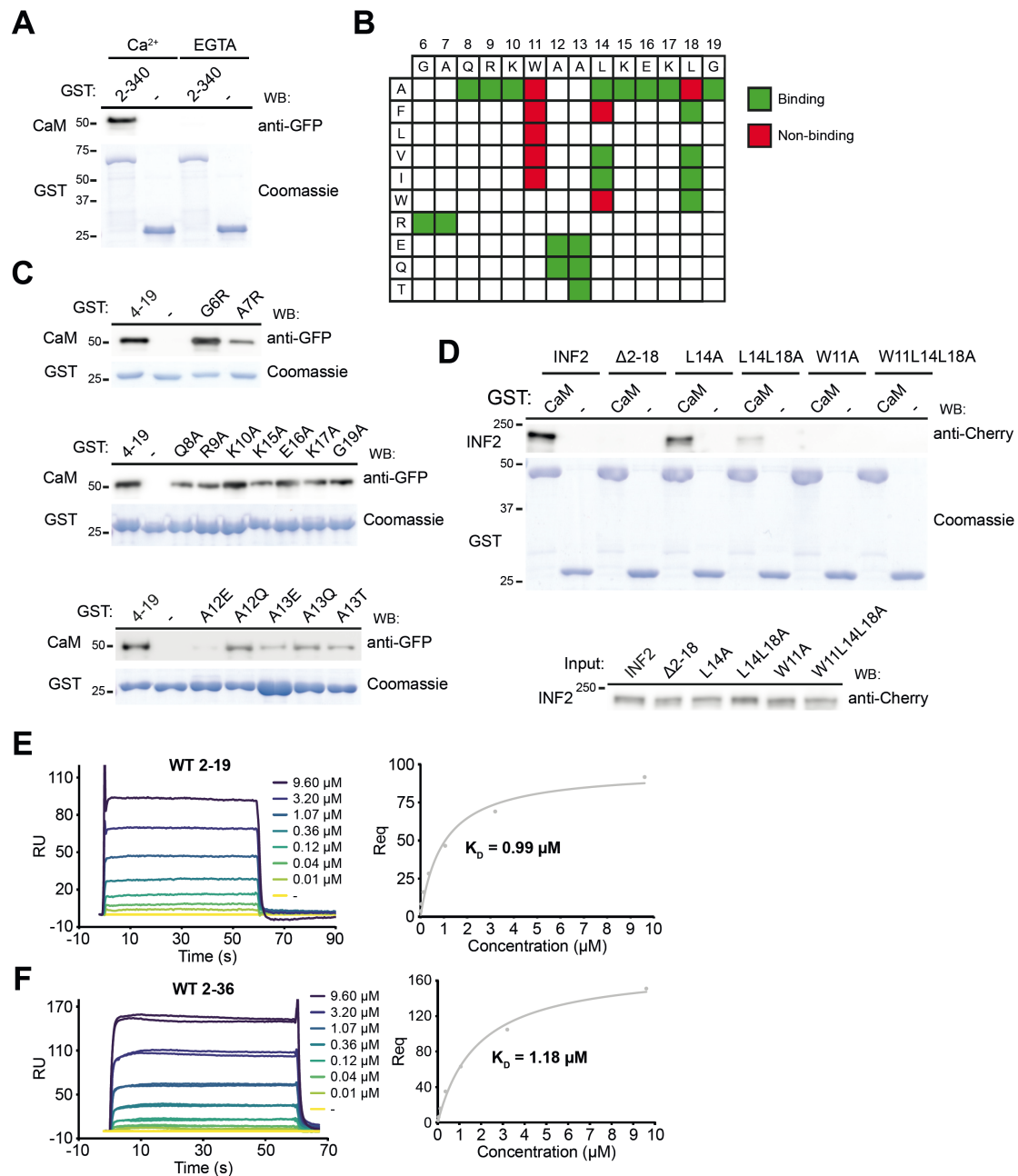


Figure S3. **Mutational analysis of the 2-19 INF2 peptide.** (A) Pull-down analysis of the association of GFP-CaM with a GST fusion of the 2-340 fragment of INF2 in the presence of 5 mM Ca^{2+} or 7.5 mM EGTA. (B) Summary of the association of GFP-CaM with GST fused to the 4-19 fragment of INF2 with the indicated amino acid replacements. (C) Representative pull-down experiments of the association of GFP-CaM with GST fusions of the intact 4-19 fragment of INF2 or with the indicated amino acid replacements. (D) A GST fusion of CaM was used in pull-down experiments with full-length INF2 either intact or with the indicated amino acid replacements. The purified GST fusions were stained with Coomassie blue as a control for the amount of GST protein used in (A, C, D). (E, F) Representative surface plasmon resonance analysis of the interaction of purified CaM from bovine testes (E) or brain (F) with immobilized 2-19 (E) or 2-36 (F) peptides in the presence of Ca^{2+} (left panels). The corresponding equilibrium plots, with indication of the apparent K_D resulting from the same experiment, are shown (right panels). RU, resonance units; Req, RU at equilibrium.

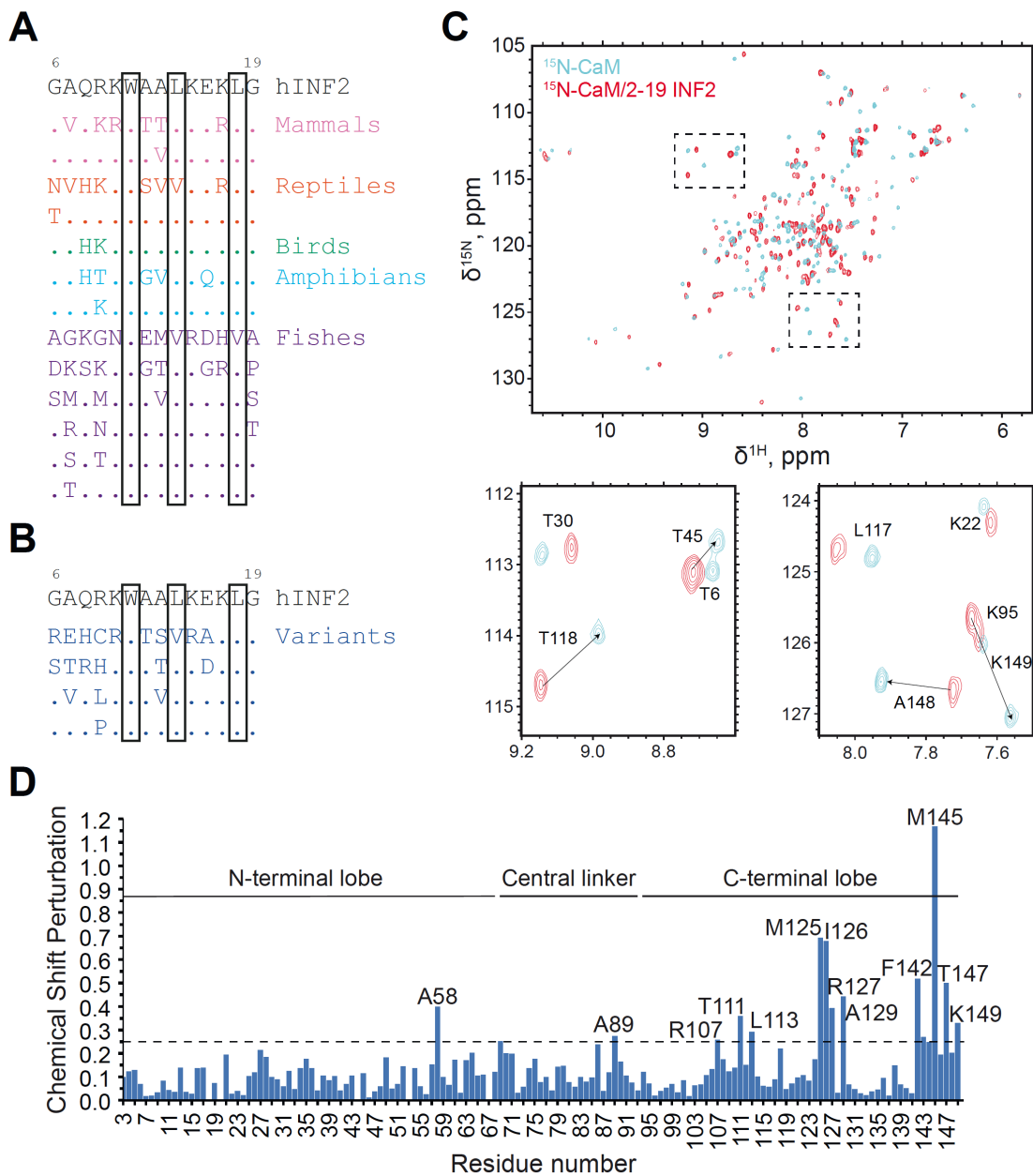


Figure S4. **Conservation of the CaM-binding motif of INF2 in vertebrates.** (A) Compilation of the amino acid replacements of the human 6-19 INF2 peptide found in more than 300 vertebrates. (B) Compilation of the amino acid replacements of the 6-19 INF2 peptide in the human population. (C) Overlay of the 2D [^1H - ^{15}N]-HSQC spectrum of the free ^{15}N -CaM (in black) and ^{15}N -CaM/2-19 INF2 at an 1:1 ratio (in red). An enlargement of the boxed regions is shown. (D) Bar plot of the averaged ^1H and ^{15}N chemical shift perturbations ($\Delta\delta^{\text{av}} = \{[(\Delta\delta_{1\text{H}})^2 + (\Delta\delta_{15\text{N}}/5)^2]/2\}^{1/2}$, ppm) as a function of the residue number of CaM. The horizontal line indicates $\Delta\delta^{\text{av}} = 0.25$ ppm, which represents the threshold. The residues above this value are indicated.

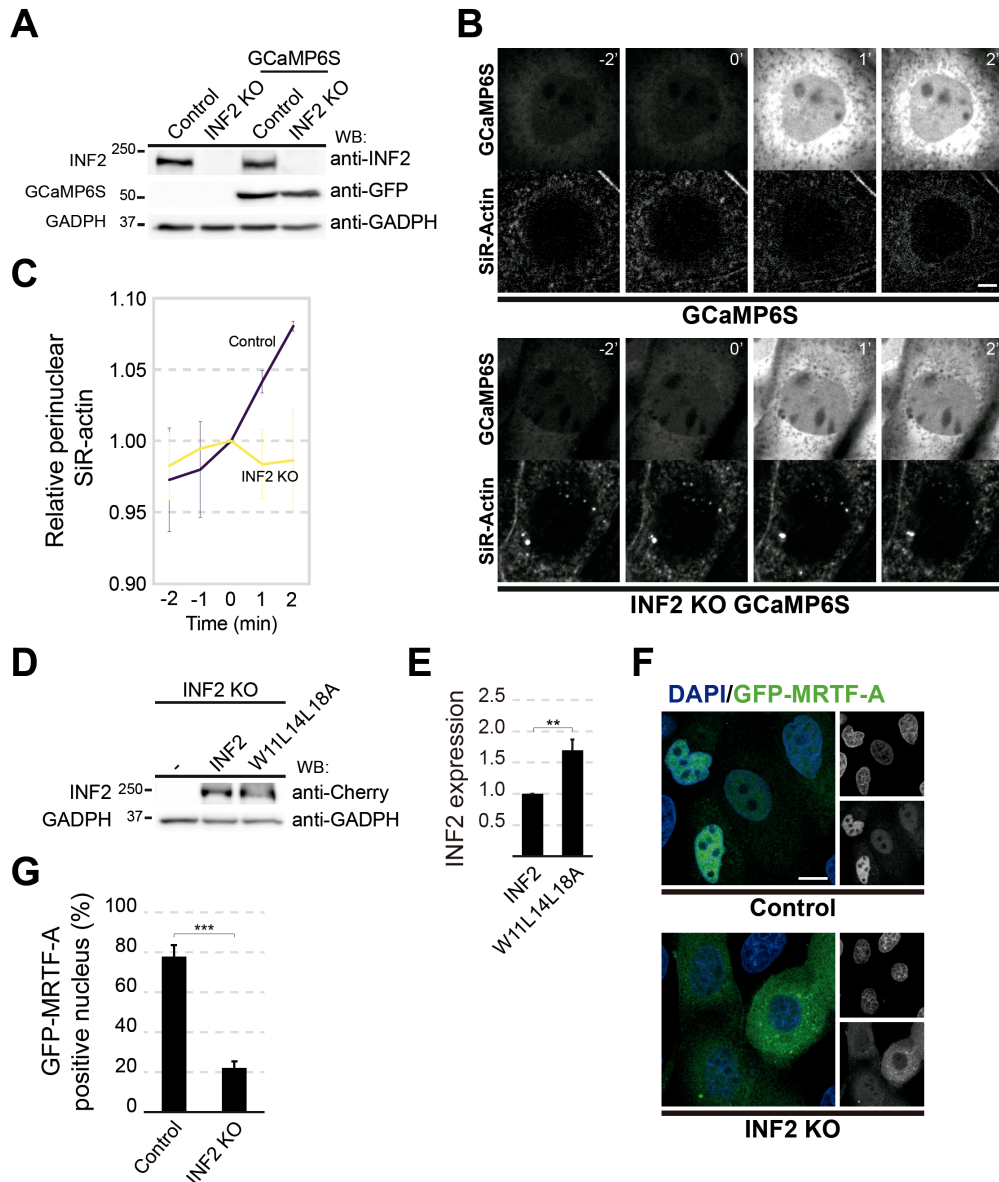


Figure S5. INF2 MDCK KO cells are defective in actin polymerization and MRTF-A translocation to the nucleus. (A) Control cells and INF2 KO cells expressing or not GCaMP6S were analyzed by immunoblotting with anti-INF2 antibodies to confirm the absence of INF2 in INF2 KO cells and with anti-GFP antibodies to analyze the levels of GCaMP6S. GADPH was used as a loading control. (B, C) Control cells and INF2 KO cells expressing GCaMP6S were incubated with SiR-actin to visualize F-actin. Cells were treated with A23187 (t = 0 min) and analyzed by videomicroscopy before and after treatment. Note that, although the staining of F-actin with SiR-Actin in live cells was poorer than that obtained with fluorescent phalloidin in fixed cells, it was useful to detect the increase of F-actin after A23187 stimulation (B). (C) Kinetics of the perinuclear content of F-actin as measured by SiR-actin fluorescence relative to that of cells at t = 0 min. Data represent the mean and SD of three independent experiments (≥ 30 cells were analyzed; three independent experiments). (D, E) The expression of exogenous INF2-1 and INF2-1 W11L14L18A in INF2 KO cells was analyzed with anti-Cherry antibodies. The levels of GAPDH were taken as a loading control (D). The graph shows the expression of exogenous INF2-1 W11L14L18A relative to that of exogenous INF2-1 (E). Three independent experiments; **, $p < 0.01$. (F, G) Representative images of control cells and INF2 KO cells transiently expressing GFP-MRTF-A after treatment with A23187 (F). (G) Histogram of percentage of cells with GFP-MRTF-A in the nucleus. The mean and SD are shown (> 350 cells were examined; three independent experiments; ***, $p < 0.001$).

Table S1. Summary of structural statistical parameters for the ensembles of the 20 lowest target function conformers calculated for peptides INF2-2-19 and INF2-2-36 in 30 %TFE at pH 5.5.

Peptide	INF2-2-19	INF2-2-36
Number of distance restraints		
Intraresidue & sequential ($i - j \leq 1$)	74	166
Medium range ($1 < i - j < 5$)	23	28
Long range ($ i - j \geq 5$)	0	0
Total number	97	194
Averaged total number per residue	5.4	5.5
Number of dihedral angle constraints		
Number of restricted ϕ angles	16	29
Number of restricted ψ angles	15	27
Total number	31	56
Pairwise RMSD (Å)		
All residues (excluding N- and C-terminal)		
	3-18	3-35
Backbone atoms	0.7±0.2	6.9±2.7
All heavy atoms	1.8±0.3	8.1±2.5
N-terminal helix 1		
	3-17	3-17
Backbone atoms	0.6±0.2	0.6±0.2
All heavy atoms	1.8±0.3	1.6±0.3
Helix 2		
	---	25-31
Backbone atoms	---	0.4±0.2
All heavy atoms	---	1.3±0.2
Ramachandran plot (%)		
Most favoured regions	98.3	89.8
Additionally allowed regions	1.7	10.2
Generously allowed regions	0.0	0.0
Disallowed regions	0.0	0.0

Table S2. List of NMR experiments acquired for ^{15}N -CaM and $^{15}\text{N},^{13}\text{C}$ -CaM

	Number of points	Spectral Width (ppm)	Number of scans	Time	NUS
Sequential Assignment of free $^{15}\text{N},^{13}\text{C}$ -CaM (25°C)					
2D ^1H - ^{15}N HSQC	2k x 256	12(^1HN) x 29(^{15}N)	4	20min	--
3D HNCO	2k x 56 x 96	12(^1HN) x 29(^{15}N) x 14(^{13}CO)	4	7.2h	--
3D HNcaCO	2k x 56 x 96	12(^1HN) x 29(^{15}N) x 14(^{13}CO)	8	14.8h	--
3D HNCA	2k x 56 x 80	12(^1HN) x 29(^{15}N) x 30(^{13}C)	4	7.2h	--
3D HNcoCA	2k x 56 x 80	12(^1HN) x 29(^{15}N) x 30(^{13}C)	8	17.8h	--
3D CBCAcoNH	2k x 56 x 96	12(^1HN) x 29(^{15}N) x 80(^{13}C)	8	15h	--
3D HNCACB	2k x 56 x 80	12(^1HN) x 29(^{15}N) x 80(^{13}C)	24	36.5h	--
Sequential Assignment of $^{15}\text{N},^{13}\text{C}$ -CaM/INF2-2-19 at ratio 1:2 (25°C)					
2D ^1H - ^{15}N HSQC	2k x 128	12(^1HN) x 29(^{15}N)	2	5min	--
3D HNCO	2k x 56 x 96	12(^1HN) x 29(^{15}N) x 14(^{13}CO)	4	1.5h	25%
3D HNCA	2k x 56 x 80	12(^1HN) x 29(^{15}N) x 30(^{13}C)	4	3.0h	50%
3D CBCAcoNH	2k x 56 x 96	12(^1HN) x 29(^{15}N) x 80(^{13}C)	8	6.5h	45%
3D HNCACB	2k x 56 x 80	12(^1HN) x 29(^{15}N) x 80(^{13}C)	24	14.3h	40%